

Teaching Tailored to Talent: Adverse Weather Restoration via Prompt Pool and Depth-Anything Constraint

Sixiang Chen¹ Tian Ye¹ Kai Zhang¹ Zhaohu Xing¹ Yunlong Lin² Lei Zhu^{1,3*}
¹The Hong Kong University of Science and Technology (Guangzhou) ²Xiamen University
³The Hong Kong University of Science and Technology

Project page: <https://ephemeral182.github.io/T3-DiffWeather>

Abstract

Recent advancements in adverse weather restoration have shown potential, yet the unpredictable and varied combinations of weather degradations in the real world pose significant challenges. Previous methods typically struggle with dynamically handling intricate degradation combinations and carrying on background reconstruction precisely, leading to performance and generalization limitations. Drawing inspiration from prompt learning and the "Teaching Tailored to Talent" concept, we introduce a novel pipeline, **T³-DiffWeather**. Specifically, we employ a prompt pool that allows the network to autonomously combine sub-prompts to construct weather-prompts, harnessing the necessary attributes to adaptively tackle unforeseen weather input. Moreover, from a scene modeling perspective, we incorporate general prompts constrained by Depth-Anything feature to provide the scene-specific condition for the diffusion process. Furthermore, by incorporating contrastive prompt loss, we ensure distinctive representations for both types of prompts by a mutual pushing strategy. Experimental results demonstrate that our method achieves state-of-the-art performance across various synthetic and real-world datasets, markedly outperforming existing diffusion techniques in terms of computational efficiency.

1. Introduction

With the growth of the community, image restoration in adverse weather conditions has become increasingly significant [17, 19, 20, 22, 40, 75, 83]. To meet practical demands effectively, research is increasingly focusing on the all-in-one removal of multiple weather degradations [21, 47, 59, 77, 88] as a primary objective.

Contrasting with restoration tasks targeted at specific weather conditions, multi-weather restoration involves a composition of various weather phenomena. Early developments employed methods such as neural architecture search [47] or distillation [21] to combine models tailored

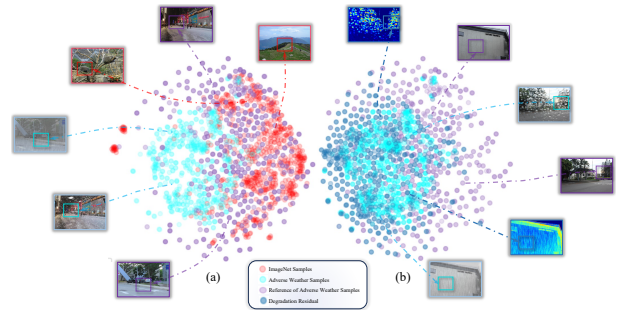


Figure 1. **t-SNE visualization of different feature distributions.** (a). Scenes with different contents also have significant commonalities compared to degradations. And there are some differences and commonalities between degradations and degradations. (b). Degradation residuals can represent degradations to a certain extent and be distinguished from the background.

to individual tasks, but these approaches are complicated and cumbersome. Moreover, several methods [77, 91] have attempted to employ a codebook as a reliable prior for guiding image restoration or utilized shared learnable queries to adapt different weather degradations. However, such paradigms are not aware of the differences and similarities between degradations. Recently, the WGWS framework [103] analyzed the weather-general and weather-specific features and performed targeted parameter learning for such characteristics. Yet, its two-stage design and the need for customized modifications within different architectures remain intricate. In addition, unlike dealing with a single weather, adverse weather will cause unseen and unpredictable degradation combinations in the real world, which poses a challenge to handling degradations adaptively. Hence, *1. How to effectively and flexibly model complicated and unpredictable weather combinations in the real world remains an open question.*

Furthermore, benefiting from recent advancements in diffusion models [29], there is the first diffusion-based method—WeatherDiffusion [59]—which has demonstrated the superiority of generative paradigms over regression models in reconstructing clean backgrounds from adverse

*Lei Zhu (leizhu@ust.hk) is the corresponding author.

weather images. However, its shortcomings are evident: the original degraded image as a condition does not adequately guide the reconstruction from noise to clean images, and requires a certain number of steps for sampling. For diffusion models, discovering sufficiently informative conditions is essential for high-quality image reconstruction [28, 43, 49, 82]. Therefore, **2. Designing a condition that equips rich information on adverse weather samples is critical for diffusion process.**

To address the aforementioned challenges, we introduce a novel paradigm. Inspired by prompt learning [33, 100], we claim that prompts can be employed to craft a comprehensive condition. **i).** Unlike the recent paradigm [60] that utilized a shared set of learnable prompts to adapt to varying degraded images, we design a prompt pool. This pool can fully exploit the differences and similarities among weather degradations, thereby offering the network a wider range of options. Specifically, we enable the network to autonomously construct the necessary weather information based on the input degradation residual and freely assemble a specific set of weather-prompts for unpredictable phenomena. **ii).** We observe that the scene features behind adverse weather often share commonalities (see Fig.1 (a)), inspiring us to devise general prompts specifically for background modeling. Drawing inspiration from the recent breakthroughs in Depth-Anything [84], we note this model exhibits exceptional robustness when handling extreme samples. This observation leads us to extract critical features from Depth-Anything, utilizing them to direct our general prompts. **iii).** Additionally, we introduce a compact contrastive prompt loss to further regulate two types of prompts, and integrate them seamlessly into the diffusion process. At the core of our approach, a "Teaching Tailored to Talent" paradigm is resembled, adeptly guiding distinct weather combinations and their respective scene backgrounds. Building upon this foundation, we introduce a novel diffusion-based architecture: *T³-DiffWeather*. It achieves SOTA performance across various adverse weather benchmarks while requiring only a tenth of the sampling steps compared to the latest WeatherDiffusion [59].

As an overview, the contributions of our work are summarized as follows:

- We introduce a novel prompt pool. Capitalizing on the similarities and differences among various weather conditions, proposed prompt pool empowers the network to autonomously combine sub-prompts, effectively constructing diverse weather-prompts to enhance representation for complicated weather degradations.
- Inspired by the shared attributes within the scenes of degraded samples, we have crafted general prompts specifically tailored for background understanding. For the first time, we propose to utilize the robust features of Depth-Anything [84] as a constraint for general prompts.

- We incorporate a compact contrastive prompt loss to further boost the prompt representation of two designs. Overall, our diffusion-based architecture, *T³-DiffWeather*, achieves SOTA performance on multi-weather restoration benchmarks with significantly fewer inference steps.

2. Related Works

2.1. Adverse Weather Restoration

Dehazing: The field of single-image dehazing has witnessed remarkable advancements in recent years [2, 51, 53, 62, 75, 80, 90]. DehazeFormer [75] adopted a transformer-based approach, tackling the complicated hazy images through distinct window processing. Meanwhile, the MB-TaylorFormer [62] leveraged a linear Transformer architecture grounded in Taylor series expansion to clarify hazy scenes effectively.

Deraining: The progress in single-image rain removal is steadily increasing, including rain streaks [22, 66, 86, 102] and raindrops [17, 61, 63, 81, 83]. IDT [83] developed a transformer-based technique that combines window-based and spatial transformers to enhance the precision of rain streak modeling. UDR-S2Former [17] leveraged uncertainty to refine the sparse ViT model for improved performance of raindrop removal.

Desnowing: Unlike dehazing and deraining, single-image snow removal presents a greater challenge [9, 15, 16, 18, 19, 24, 50, 89]. JSTASR [19] introduced a framework capable of addressing both haze and snow removal simultaneously. MSP-Former [16] was the inaugural attempt at a single-image snow removal network utilizing a transformer architecture. Nevertheless, similar to haze and rain removal, these innovative approaches still grapple with limitations when confronted with other variants of extreme weathers.

Multi-Weather Restoration: Adverse weather restoration endeavors to develop a consolidated network to adeptly address weather-induced image degradations [21, 47, 59, 77, 87, 91, 103]. The pioneering work in this domain was the All-in-One [47], the extensive parameterization due to NAS may make it impractical for real-world deployment. TransWeather [77] introduced a weather-type decoder capable of interpreting diverse weather degradations, yet its fixed queries cannot explicitly consider the degradations of different weather and lacks background-level modeling. WeatherDiffusion [59] presented a diffusion-based method that harnessed the capabilities of diffusion models for weather removal, achieving SOTA results across various benchmarks. Nonetheless, the slow inference speed and the absence of precise prompt conditions may hinder its widespread practical application.

2.2. Conditional Diffusion Models

Recent advancements in denoising diffusion probabilistic models (DDPM) [30] have captured intricate distributions

with accuracy that exceeds other generative frameworks, including GANs. To further enhance the precision and realism of the generated outputs, diffusion models often incorporated additional conditioning or guidance mechanisms, as evidenced by recent studies [3, 4, 27, 38]. In the field of image restoration, the prevailing approach involves feeding networks with concatenated degraded inputs to yield outputs of high fidelity quality [43, 44, 59, 69, 92] compared with traditional regressive models [26, 36, 39, 41, 42, 67, 79]. To further refine the denoising process, networks often incorporated single task-specific prompts such as masks or textual information [28, 85] as embedded guidance. However, the recent WeatherDiffusion [59] typically used degraded images as the sole condition, which may result in performance limitations for addressing all-in-one restoration tasks.

2.3. Prompt Learning

Prompt learning has been increasingly applied to computer vision [6, 7, 58, 71, 72, 97]. This technique involved the insertion of task-specific prompt tokens prior to the input, equipping pre-trained models with the necessary knowledge to perform new tasks without extensive fine-tuning. The approach of Context Optimization (CoOp)[100] leveraged this for the CLIP model[65], refining prompts in a continuous space through backpropagation. Conditional Context Optimization (CoCoOp)[99] innovated further by producing input-dependent prompt residuals to enhance generalization ability. For low-level tasks, PromptIR [60] introduced a learnable prompt module that generates shared prompts responsive to various degradation types. Additionally, recent researches utilized text prompts to guide image restoration networks [23, 49, 76]. However, the use of sparse text embeddings could lead to performance limitations and increase complexity due to the necessity for additional multi-modal models.

3. Preliminaries

Diffusion Models. Diffusion models (DMs) [29, 56] infuse training data with Gaussian noise and then recover the original data through the inversion of this noise. Initially, DMs implement a diffusion algorithm that incrementally converts a starting image \mathbf{x}_0 into a noise distribution $\mathbf{x}_T \sim \mathcal{N}(0, 1)$ across T steps. Each step of this transformation is described by the equation:

$$q(\mathbf{x}_t|\mathbf{x}_{t-1}) = \mathcal{N}\left(\mathbf{x}_t; \sqrt{1 - \beta_t}\mathbf{x}_{t-1}, \beta_t\mathbf{I}\right), \quad (1)$$

with \mathbf{x}_t representing the image with noise at timestep t , β_t as a predetermined scale parameter, and \mathcal{N} signifying the Gaussian distribution. Defining $\alpha_t = 1 - \beta_t$ and $\bar{\alpha}_t = \prod_{i=0}^t \alpha_i$ allows us to simplify Eq.1 as:

$$q(\mathbf{x}_t|\mathbf{x}_0) = \mathcal{N}\left(\mathbf{x}_t; \sqrt{\bar{\alpha}_t}\mathbf{x}_0, (1 - \bar{\alpha}_t)\mathbf{I}\right). \quad (2)$$

During the inference phase, DMs commence by generating a Gaussian noise map \mathbf{x}_T and then progressively apply a denoising process until reaching a high-fidelity result \mathbf{x}_0 :

$$p(\mathbf{x}_{t-1}|\mathbf{x}_t, \mathbf{x}_0) = \mathcal{N}\left(\mathbf{x}_{t-1}; \boldsymbol{\mu}_t(\mathbf{x}_t, \mathbf{x}_0), \sigma_t^2\mathbf{I}\right), \quad (3)$$

where the mean value $\boldsymbol{\mu}_t(\mathbf{x}_t, \mathbf{x}_0) = \frac{1}{\sqrt{\alpha_t}}\left(\mathbf{x}_t - \epsilon\frac{1-\alpha_t}{\sqrt{1-\bar{\alpha}_t}}\right)$ and the variance $\sigma_t^2 = \frac{1-\bar{\alpha}_{t-1}}{1-\bar{\alpha}_t}\beta_t$. The noise estimate ϵ is optimized $\epsilon_\theta(\mathbf{x}_t, t)$ through training as follows: with a clean image \mathbf{x}_0 , DMs select a random timestep t and noise $\epsilon \sim \mathcal{N}(0, \mathbf{I})$ to produce the noisy images \mathbf{x}_t as per Eq.2. DMs then optimize the model parameters θ of ϵ_θ in accordance with [29]:

$$\mathcal{L}_{diff} = \mathbb{E} \left\| \epsilon - \epsilon_\theta\left(\sqrt{\bar{\alpha}_t}\mathbf{x}_0 + \epsilon\sqrt{1 - \bar{\alpha}_t}, t\right) \right\|_2^2. \quad (4)$$

4. Methods

Novel Pipeline T³-DiffWeather. For adverse weather restoration, the intricate blend of degradations in the real world poses significant challenges to obtaining clean backgrounds. Consequently, developing a model that can effectively adapt complicated degradation combinations is crucial. We introduce a novel pipeline, T³-DiffWeather, whose key principle is “Teaching Tailored to Talent.” Inspired by prompt learning [33, 60, 100], our design incorporates instance-wise weather-prompts tailored for specific degradations and general prompts for scene information, efficiently exploiting both the disparate and shared attributes present in degraded images. We leverage these prompts as the condition to guide the diffusion process with rich information.

Specifically, leveraging insights from Fig.1, we observe that degradations exhibit more distinct features compared to the background (as shown in Fig.1(a)), and degradation residual \mathbf{r}_d (subtract the degraded image \mathbf{y} from the clean image \mathbf{x}) provides a clearer representation of the degraded image (as illustrated in Fig.1(b)). We claim that the degradations are a primary factor for the difficulty in restoration. Therefore, we pivot the reconstruction target of the diffusion model toward the degradation residual. The training objective is changed to follows compared with Eq.4:

$$\mathcal{L}_{res} = \mathbb{E} \left\| \epsilon - \epsilon_\theta\left(\underbrace{\sqrt{\bar{\alpha}_t}(\mathbf{x} - \mathbf{y})}_{\text{residual } \mathbf{r}_d} + \sqrt{1 - \bar{\alpha}_t}\epsilon, \mathbf{y}, \mathbf{c}\right) \right\|_2^2. \quad (5)$$

where \mathbf{c} denotes the condition built by weather-prompts \mathcal{P}_w and general prompts \mathcal{P}_{gd} . We simply embed them into the latent layer in the diffusion network through cross-attention, similar to the text embedding in SD [68]. This process is naturally efficient and does not take up much computation

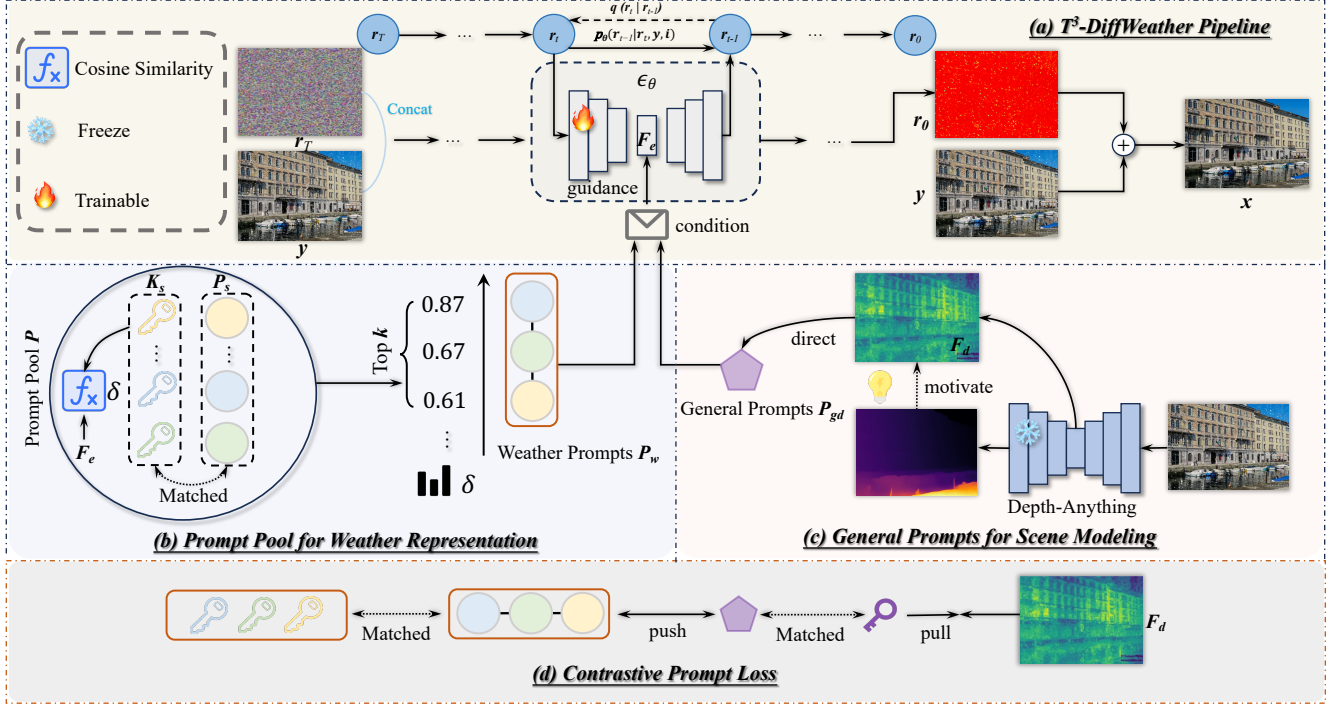


Figure 2. **The overview of proposed method.** (a) showcases our pipeline, which adopts an innovative strategy focused on learning degradation residual and employs the information-rich condition to guide the diffusion process. (b) illustrates the utilization of our prompt pool, which empowers the network to autonomously select attributes needed to construct adaptive weather-prompts. (c) depicts the general prompts directed by Depth-Anything constraint to supply scene information that aids in reconstructing residuals. (d) shows the contrastive prompt loss, which exerts constraints on prompts driven by two distinct motivations, enhancing their representations.

overhead. Given the feature embedding $\mathcal{F}_e \in \mathbb{R}^{H \times W \times D}$ in the latent layer, The formula can be expressed as follows:

$$\begin{aligned} \mathcal{F}'_e &= \text{softmax} \left(\frac{\mathcal{Q}(\mathcal{F}_e) \mathcal{K}(\mathcal{P}_w)^T}{\sqrt{D}} \right) \mathcal{V}(\mathcal{P}_w), \\ \hat{\mathcal{F}}_e &= \text{softmax} \left(\frac{\mathcal{Q}(\mathcal{F}'_e) \mathcal{K}(\mathcal{P}_{gd})^T}{\sqrt{D}} \right) \mathcal{V}(\mathcal{P}_{gd}), \end{aligned} \quad (6)$$

where $\mathcal{Q}(\cdot)$, $\mathcal{K}(\cdot)$, $\mathcal{V}(\cdot)$ are the query, key, and value functions. The $\hat{\mathcal{F}}_e$ is the output feature embedding.

4.1. Prompt Pool for Weather Representation

Motivation I: The restoration from adverse weather is often impeded by the complicated and varied combinations of degradations, which can influence network performance. Unlike the substantial domain gap encountered in general restoration between various types of degradations [8, 10, 96], weather degradations in the real world exhibit some similar attributes, such as haze veiling and low contrast [103]. Concurrently, degradations specific to distinct conditions manifest unique attributes varying in shape and scale. These differences and similarities inspire us to explicitly leverage degradation characteristics to enhance the representation of degradations.

Leveraging the advancements in prompt learning for image restoration, we posit that the network should adaptively

learn the characteristics of degradations and autonomously construct suitable weather-prompts. Consequently, we introduce the design of a prompt pool. This design triggers the network to selectively choose sub-prompts from the pool, crafting a unique weather-prompt tailored to each sample. Such an autonomous construction explicitly takes into account the similarities (shared sub-prompts) and differences (independent sub-prompts) under varying weather conditions. Specifically, given our prompt pool $\mathcal{P} = \{\mathcal{P}_s^i\}_{i=1}^N$ with each sub-prompts $\mathcal{P}_s^i \in \mathbb{R}^{L_s \times D}$ (L_s denotes the length of tokens), where i represents the index of a specific sub-prompts and N is the prompt pool size. For the input (degradation residual) embedding \mathcal{F}_e , the weather-prompt construction function Ψ can be defined as:

$$\mathcal{P}_w = \Psi(\mathcal{P}, \mathcal{F}_e; \Theta), \quad (7)$$

Here, Θ parameterizes the selection process to optimally align the sub-prompts with the embedded feature (related to degradation) \mathcal{F}_e . Motivated by the essence of ViT [25], we utilize the query-key mechanism, which enables the network to select the necessary sub-prompts for the input embedding. Specifically, a learnable key $\mathcal{K}_s^i \in \mathbb{R}^{1 \times D}$ is designed for each sub-prompts to calculate the correlation with embedding \mathcal{F}_e (query) for choose. The formula can be expressed as follows:

Selection Frequency of Sub-Prompts for Different Tasks

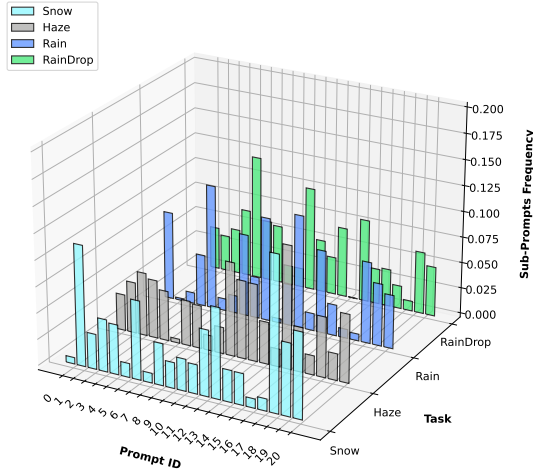


Figure 3. **The selection frequency of sub-prompts.** Some similar selection frequencies reflect the network’s ability to adaptively exploit common attributes in some similarity between tasks (e.g. rain and raindrop). At the same time, the unique prompt frequencies highlight the flexibility to adapt to the specific characteristics of each weather condition.

$$\mathcal{K}_s^i \xleftrightarrow{\text{match}} \mathcal{P}_s^i, \quad \mathcal{F}_e \in \mathbb{R}^{H \times W \times D} \xrightarrow{\text{mean}} \mathcal{F}_e^{\text{mean}} \in \mathbb{R}^{1 \times D},$$

$$\delta(\mathcal{K}_s^i, \mathcal{F}_e), \quad (8)$$

where $\delta(\cdot)$ denotes the similarity calculation (we empirically choose cosine similarity). We employ this metric to let the network select the most appropriate sub-prompts from the pool to form effective weather-prompts.

$$\mathcal{P}_w = \bigcup_{i=1}^k \mathcal{K}_s^i \quad \text{if } \delta(\mathcal{K}_s^i, \mathcal{F}_e) \geq \delta(\mathcal{K}_s^{i+1}, \mathcal{F}_e), \quad (9)$$

where k is the number of sub-prompts with the top- k similarity we selected. $\bigcup_{i=1}^k$ denotes the concatenation of individual sub-prompts to construct the weather-prompts \mathcal{P}_w , which embodies the most representative features of the input in relation to the given weather conditions. Such a manner can be understood as the network using sub-prompts to freely control the weather attributes that need to be learned (see Fig.3), which is novel and efficient compared to previous paradigms. Additionally, through t-SNE visualization of the weather-prompts under distinct weather scenarios, as illustrated in Fig.4, it is evident that our constructed weather-prompts not only preserve the unique attributes of each weather type but also leverage the commonalities and differences among them. This adaptive combination tailored to individual samples achieves exceptional performance, aligning with the concept of ”teaching tailored to talent”.

Discussion I: Recently, prompt learning has been used in image restoration [60]. Nonetheless, such an approach often relied on shared parameters to address various degrada-

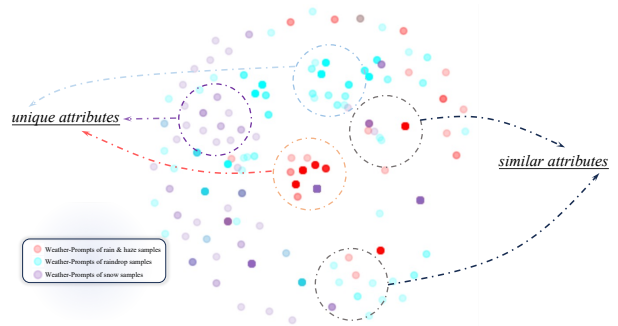


Figure 4. **t-SNE visualization of weather-prompts for different weather conditions.**

tion scenarios, leading to potential interference among different degradations and overlooking the unique features of instance-wise degradations. We aim to implement a novel strategy ”prompt pool”. It enables the network to adaptively select appropriate sub-prompts in response to the specific degradation present in the input, thereby concentrating on the inter-attributes and intra-attributes of the weather degradations.

4.2. General Prompts for Scene Modeling

Motivation II: Scene information provides guidance for the reconstruction of degraded residuals. In contrast to previous methods that solely focus on understanding degradations [59, 77, 103], we claim that modeling the scene content is another critical factor in enhancing performance. Inspired by this insight, we contemplate whether clean backgrounds in degraded images possess distinguishable characteristics. Utilizing t-SNE for visualization, we observe the distribution among clean images in Fig.1. There is often a significant distinction between degradations and background, while clean images share commonalities within the latent space. Consequently, we propose general prompts that encourage the network to boost representation with respect to the background.

The proposed general prompts $\mathcal{P}_g \in \mathbb{R}^{L_g \times D}$, unlike the degradation-specific sub-prompts, are designed to encapsulate the common attributes of the scene across various weather distortions. It serves as a versatile anchor within the representational space, fostering a consistent perception of the background. Therefore, for the initialization of prompts, we seek to impose an explicit constraint that directs the learning towards the general attributes of the scenes. It will ensure that the general prompts are not disturbed by the varying degrees of degradations.

Observation: Inspired by scene understanding [13, 34], utilizing depth information has proven to effectively represent clean scenes. Additionally, adverse weather conditions is notably more susceptible to depth-related distortions compared to other degradations. Recently, the Depth-Anything [84] model leverages extensive datasets and the robust representational capabilities of DINOv2 [57] to de-

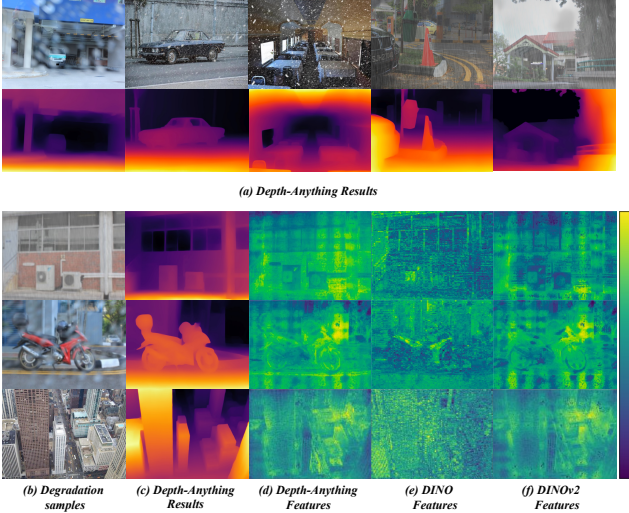


Figure 5. **Motivation of Depth-Anything [84] as a constraint.** Depth-Anything has degradation-independent performance, and the intermediate features have better robustness than the previous pre-trained network [5, 57].

velop a depth estimation model that applies to any scene. As illustrated in

Fig.5 (a), we observe that depth maps estimated by Depth-Anything are almost unaffected by degradations, which to some extent demonstrates the robustness of the intermediate hidden features in scene representation (Fig.5 (b)). Motivated by this discovery, we claim that the latent space features can be used to impose an explicit constraint on the general prompts, thereby better focusing on the background portion.

Depth-Anything Constraint: To direct the general prompts $\mathcal{P}_g \in \mathbb{R}^{L_g \times D}$ towards a more nuanced perceiving of the background, we integrate the latent features from the Depth-Anything model using an attention-based mechanism. Specifically, we define a cross-attention operation where the general prompts form the queries, and the keys and values are derived from the Depth-Anything features. Let $\mathcal{F}_d \in \mathbb{R}^{H \times W \times D}$ represents the depth-aware features, where H and W are the dimensions of the feature map. The cross-attention mechanism is then given by:

$$\mathcal{P}_{gd} = \text{softmax} \left(\frac{\mathcal{Q}_g \mathcal{K}_d^T}{\sqrt{D}} \right) \mathcal{V}_d, \quad (10)$$

Obtained general prompts \mathcal{P}_{gd} adaptively integrate scene information, providing sufficient prior knowledge for the subsequent perception of the background while mitigating the impact of degradations.

4.3. Contrastive Prompt Loss

The sections above illustrate two types of prompts as the condition for the diffusion model. Additionally, we introduce contrastive prompt loss. It aims to differentially enhance the representations of two uniquely designed

prompts. These prompts act as conditions for the diffusion model, with one tailored to model weather degradations and the other, guided by the Depth-Anything model, to perceive the background information. Given the inherently different design objectives of each prompt type, they are hypothesized to act as negative samples for each other. For the positive samples of prompt type, we employ cosine similarity to draw them nearer to the constraint within the latent space. The contrastive prompt loss \mathcal{L}_{cp} is defined as:

$$\mathcal{L}_{cp} = \frac{1}{b} \frac{1}{k} \sum_{j=1}^b \sum_{i=1}^k [\gamma(\mathcal{K}_{gd}, \mathcal{F}_d^{mean}) - \gamma(\mathcal{K}_s^i, \mathcal{K}_{gd})], \quad (11)$$

where b is the batch size. \mathcal{K}_{gd} represents the learnable key matched for general prompts, $\gamma(\cdot)$ denotes the $1 - \delta(\cdot)$, which ensures the optimization process.

Discussion II: While our approach draws inspiration from prior contrastive learning paradigms [21, 80, 98], it is distinctly different. 1). We do not require the construction of additional negative samples, as the two types of motivation-driven prompts within our design naturally serve as negatives for each other. 2). Prompts has explicit constraints that draw them closer to feature embeddings, eliminating the need for ground truth images as positive samples. 3). Our prompts can interact with high-dimensional features within the network directly, obviating the process for the traditional contrastive learning step of mapping via a pre-trained network [70] to a feature space.

4.4. Loss Function

To supervise our T³-DiffWeather model, we employ the noise estimation loss Eq.5 and the contrastive prompt loss Eq.11 during the noise estimation phase. Additionally, our contrastive prompt loss is designed to optimize the prompts adapted to different instance samples. Hence, during the training, we conduct the sampling process for restoring clean images and impose additional supervision on this process through reconstruction loss and contrastive prompt loss. This approach better constrains the optimization trajectory [31, 35] of the diffusion process and releases the potential of prompts. The overall objective function can be expressed as follows:

$$\mathcal{L}_{total} = \lambda_1 \mathcal{L}_{res} + \lambda_2 \mathcal{L}_{cp} + \lambda_3 \left\| (\mathbf{r}_d^{sample} + \mathbf{y}) - \mathbf{x} \right\|_{\text{psnr}} + \lambda_4 \mathcal{L}_{cp}^{sample} \quad (12)$$

where psnr denotes the PSNR loss [11, 14] we choose empirically. $\lambda_1, \lambda_2, \lambda_3$ and λ_4 are set to 1 empirically.

5. Experiments

5.1. Implementation

Pipeline implementation. T³-DiffWeather builds upon the backbone followed by previous diffusion design [55].

Table 1. Desnowing.

Method	Snow100K-S [50]		Snow100K-L [50]	
	PSNR \uparrow	SSIM \uparrow	PSNR \uparrow	SSIM \uparrow
SPANet _[CVPR'19] [78]	29.92	0.8260	23.70	0.7930
JSTASR _[ECCV'20] [19]	31.40	0.9012	25.32	0.8076
RESCAN _[ECCV'18] [48]	31.51	0.9032	26.08	0.8108
DesnowNet _[TIP'18] [50]	32.33	0.9500	27.17	0.8983
DDMSNet _[TIP'21] [95]	34.34	0.9445	28.85	0.8772
MPRNet _[CVPR'21] [93]	34.97	0.9457	29.76	0.8949
NAFNet _[ECCV'22] [12]	34.79	0.9497	30.06	0.9017
Restormer _[CVPR'22] [94]	35.03Δ	0.9487Δ	30.52Δ	0.9092Δ
All-in-One _[CVPR'20] [47]	-	-	28.33	0.8820
TransWeather _[CVPR'22] [77]	32.51	0.9341	29.31	0.8879
TKL&MR _[CVPR'22] [21]	34.80	0.9483	30.24	0.9020
WeatherDiff ₆₄ _[PAMI'23] [59]	35.83	0.9566	30.09	0.9041
WeatherDiff ₁₂₈ _[PAMI'23] [59]	35.02	0.9516	29.58	0.8941
AWRCP _[ICCV'23] [91]	<u>36.92</u>	<u>0.9652</u>	<u>31.92</u>	<u>0.9341</u>
★ T ³ -DiffWeather (Ours)	37.51	0.9664	32.37	0.9355

Table 2. Deraining & Dehazing.

Method	Outdoor-Rain [45]	
	PSNR \uparrow	SSIM \uparrow
CycleGAN _[ICCV'17] [101]	17.62	0.6560
pix2pix _[ICCV'17] [32]	19.09	0.7100
HRGAN _[CVPR'19] [46]	21.56	0.8550
PCNet _[TIP'21] [37]	26.19	0.9015
MPRNet _[CVPR'21] [93]	28.03	0.9192
NAFNet _[ECCV'22] [12]	29.59	0.9027
Restormer _[CVPR'22] [94]	29.97Δ	0.9215Δ
All-in-One _[CVPR'20] [47]	24.71	0.8980
TransWeather _[CVPR'22] [77]	28.83	0.9000
TKL&MR _[CVPR'22] [21]	29.92	0.9167
WeatherDiff ₆₄ _[PAMI'23] [59]	29.64	0.9312
WeatherDiff ₁₂₈ _[PAMI'23] [59]	29.72	0.9216
AWRCP _[ICCV'23] [91]	<u>31.39</u>	<u>0.9329</u>
★ T ³ -DiffWeather (Ours)	31.99	0.9365

Table 3. Raindrop Removal.

Method	RainDrop [61]	
	PSNR \uparrow	SSIM \uparrow
pix2pix _[ICCV'17] [32]	28.02	0.8547
DuRN _[CVPR'19] [52]	31.24	0.9259
RaindropAttn _[ICCV'19] [64]	31.44	0.9263
AttentiveGAN _[CVPR'18] [61]	31.59	0.9170
CCN _[CVPR'21] [63]	31.34	0.9286
IDT _[PAMI'22] [83]	31.87	0.9313
UDR-S ² Former _[ICCV'23] [17]	32.64Δ	0.9427Δ
All-in-One _[CVPR'20] [47]	31.12	0.9268
TransWeather _[CVPR'22] [77]	30.17	0.9157
TKL&MR _[CVPR'22] [21]	30.99	0.9274
WeatherDiff ₆₄ _[PAMI'23] [59]	30.71	0.9312
WeatherDiff ₁₂₈ _[PAMI'23] [59]	29.66	0.9225
AWRCP _[ICCV'23] [91]	<u>31.93</u>	<u>0.9314</u>
★ T ³ -DiffWeather (Ours)	32.66	0.9411

Figure 6. These tables provide quantitative comparisons with state-of-the-art image desnowing, deraining, and adverse weather removal methods, employing PSNR and SSIM as metrics—where higher values signify better restoration. The best and second-best metrics are shown with **bold text** and underlined text, respectively. The triangle Δ represents the SOTA metric trained on a single dataset. Above half of the tables present comparisons of task-specific methods for a single dataset, while the bottom section showcases the performance of the proposed T³-DiffWeather method across all four test sets against state-of-the-art adverse weather solutions, including All-in-One [47], TransWeather [77], TKL&MR [21], WeatherDiffusion [59] and AWRCP [91].

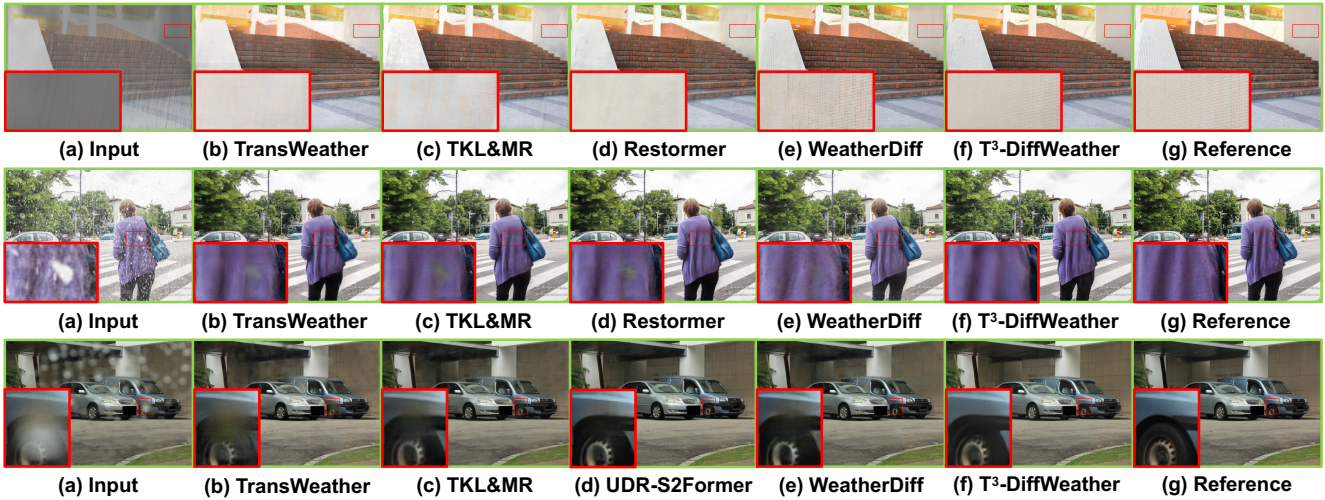


Figure 7. Visual comparisons in adverse weather conditions on Snow100K [50], Outdoor-Rain [77] and RainDrop [61] datasets.

We employ uniform initialization techniques to set up the weights for sub-prompts in the prompt pool and general prompts, including their respective keys. Specifically, we designate a total of 20 sub-prompts within the prompt pool, with each sub-prompt comprising 64 tokens (L_s), from which we select the top 5 (k) to form the required weather-prompts. The token number for general prompts (L_g) is set at 256 to ensure the balance between performance and manageable overhead. When constraining the general prompts using Depth-Anything [84], we utilize the ViT-S architecture, which demands minimal memory usage while maintaining robustness. During the diffusion process, we opt for DDIM [73] sampling. Owing to our focus on reconstructing degradation residuals and the rich representations of the condition, setting the number of sampling steps to merely

2 suffices to achieve impressive performance. Additional architectural details can be found in the supplementary materials.

Training details. To train our T³-DiffWeather model, we leverage the comprehensive AllWeather dataset referenced in [77], including 18,069 images from the Snow100K [50], Outdoor-Rain [45], and RainDrop [61] datasets, the same as previous adverse weather restoration methods [47, 59, 77, 91]. Our T³-DiffWeather pipeline is developed on the PyTorch framework and undergoes training on two NVIDIA A800 GPUs. This pipeline includes 800K training iterations, utilizing the Adam optimizer with momentum parameters set to 0.9 and 0.995. Training commences with an initial learning rate of 1.5×10^{-4} , which is reduced using a cosine annealing schedule. To promote stability during

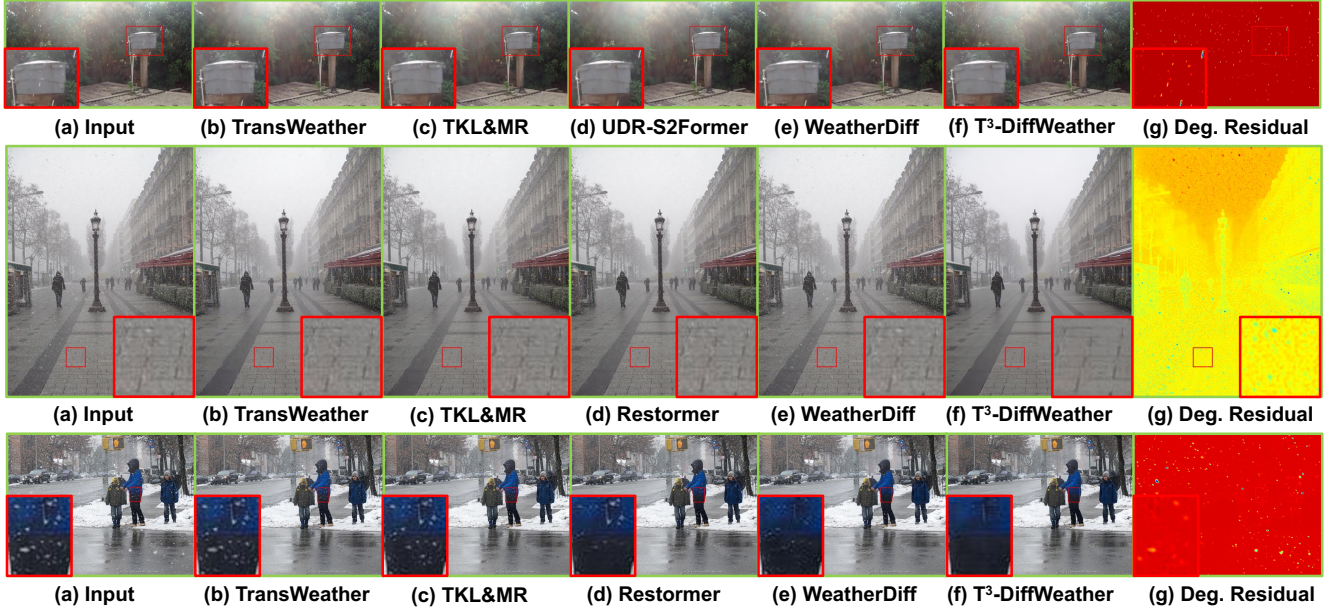


Figure 8. Visual comparisons of the real-world adverse weather samples.

the learning phase, an exponential moving average strategy weighted at 0.995 is employed for parameter updates, as supported by findings in [56] and [74]. The diffusion procedure consists of 1,000 timesteps, labeled as T , with an incrementally ascending noise schedule β_t ranging from 0.0001 to 0.02. The training employs image patches of 256×256 pixels. Augmentation techniques like horizontal flipping and fixed-angle random rotation are used in the training. Please refer to the supplementary material to view detailed training and testing dataset configurations.

5.2. Quantitative comparison

We perform a comparative analysis of metrics between synthetic and real datasets. Specifically, we compare the model performance for a single task and the performance of a multi-weather image restoration model trained on multiple weather datasets. Our quantitative analysis reveals the competitive advantage of our T³-DiffWeather pipeline over existing state-of-the-art algorithms in image restoration with various weather impacts. As shown in Tab.1, T³-DiffWeather achieves excellent performance in image snow removal, as evidenced by the highest PSNR and SSIM metrics on the Snow100K-S [50] and Snow100K-L [50] datasets. It is particularly noteworthy that the PSNR on Snow100K-S is 1.68db higher than the previous best diffusion model, WeatherDiffusion [59], indicating a significant improvement in recovery quality. This is mainly due to our new pipeline design and suitable and effective conditions. In addition, our method ranks first in the deraining and de-hazing task (Tab.2) and maintains the leading position in the raindrop removal (Tab.3).

5.3. Visual Comparison

Fig.7 visually compares state-of-the-art image restoration techniques on a synthetic dataset designed to simulate real-world conditions. WeatherDiffusion [59] marginally enhances detail definition but does not remove degradations entirely in some areas. Restormer improves color fidelity but does not entirely eliminate synthetic artifacts. T³-DiffWeather, our method, markedly improves texture and color accuracy, closely matching the reference. It significantly reduces synthetic distortions, maintaining scene authenticity, as seen in the detailed insets.

Furthermore, Fig.8 also shows a visual comparison of restoration methods applied to images of real-world scenarios. Also based on a diffusion model, our method can better remove degradation in the real world and restore complex scene textures than WeatherDiffusion [59]. In addition, UDR-S2Former [17] has deficiencies in handling real rainy scenes. In comparison, our method visually removed all degradations details, which proves the competitiveness of our method compared to specific methods. We also show the heat map of our degradation residual. We find that our method always focuses on degradations in terms of the restoration object, which proves the effectiveness of our pipeline.

6. Evaluating Real-World Performance

To further demonstrate the superiority of our paradigm in the real world, we conduct a quantitative comparison of real-world datasets. Tab.4 presents an evaluation of our T³-DiffWeather approach on datasets captured under real-world meteorological conditions [1, 17, 63]. Our T³-

Table 4. Com. on more datasets.

Method	RainDS-Real(RDS)		GT-RAIN	
	PSNR \uparrow	SSIM \uparrow	PSNR \uparrow	SSIM \uparrow
WGWS-Net [103]	20.79	0.603	20.65	0.608
WeatherDiff ₁₂₈ [59]	21.09	0.605	20.83	0.613
AWRCP [91]	21.31	0.607	20.97	0.615
★ T ³ -DiffWeather (ours)	21.96	0.612	21.27	0.619

DiffWeather method achieves impressive scores, emphasizing its excellent adaptability to different environmental conditions. This shows that our "teaching tailored to talent" paradigm can allow the network to adaptively utilize the required attributes, which is effective for diverse real-life scenarios. It shows that our method is widely applicable to actual environments.

6.1. Comparison of Parameters and Complexity

Table 5. Com. of parameters and GFLOPs (256×256 resolution) for diffusion process and the regressive model.

Method	#Params	#GFLOPs
Image Restoration (Regression)		
Restormer [94]	25.3M	140.92G
Image Restoration (Diff)		
IR-SDE [54]	135.3M	119.1G×100 steps
Refusion [55]	131.4M	63.4G×50 steps
Adverse Weather Restoration (Diff)		
WeatherDiffusion [59]	113.68M	248.4G×25 steps
T ³ -DiffWeather (ours)	69.38M	59.82G×2 steps

As shown in Tab.5, our pipeline significantly reduces the number of parameters required for diffusion compared to previous designs, while decreasing the GFLOPs compared with the regressive model [94]. Moreover, with only two steps in the sampling process, the computational complexity at a 256×256 resolution is a mere **1/52** of that of the SOTA WeatherDiffusion [59]. Additionally, the computational complexity of the single image restoration diffusion architecture Refusion [55] is nine times of ours, underscoring the efficacy of proposed conditions and constraints and the superiority of our holistic approach aimed at reconstructing degradation residuals.

6.2. Ablation Studies

In order to verify the efficacy of each key component of T³-DiffWeather, we conduct a series of ablation experiments. All these variants are trained using the same configurations as in the implementation details, and the ablation results are tested on Outdoor-Rain [45].

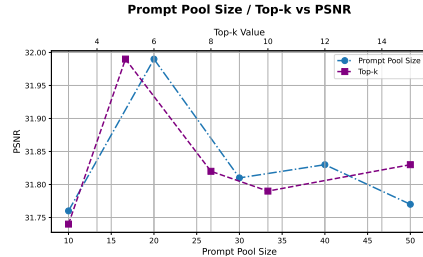
Table 6. Abl. of Prompt Pool.

Method	PSNR \uparrow	SSIM \uparrow
w/o. prompt pool	31.05	0.9325
w/o. matched keys	31.72	0.9349
w. prompt [60]	31.38	0.9330
w. prompt pool (Ours)	31.99	0.9365
Length L_s	PSNR \uparrow	SSIM \uparrow
32 (Sub-prompts)	31.79	0.9358
64 (Sub-prompts) (Ours)	31.99	0.9365
128 (Sub-prompts)	32.04	0.9366

the advances in prompt learning, our prompt pool method autonomously crafts tailored sub-prompts for each specific

Effectiveness of Prompt Pool. The Tab.6 highlight the vital role of the proposed prompt pool in adverse weather restoration. Leveraging

degradation scenario. This approach has shown substantial improvements over methods without a prompt pool or with unmatched keys and significantly surpasses the previous design [60]. With our method, the network selects the most representative sub-prompts with 64 token numbers of sub-prompts to balance the complexity and performance, affirming the prompt pool’s utility in capturing the attributes of complex weather patterns.

Figure 9. Abl. of Prompt pool size and k value of top- k .

Discussion of prompt pool size and topk. Our results show that as the prompt pool size increases, the model has sufficient diversity in prompts to effectively capture and represent various degraded properties. Conversely, a prompt pool that is too large may introduce redundancy or noise, thereby compromising the model’s resilience. Additionally, for top- k , too fine-grained selection may lead to overfitting of poorly represented degradation attributes or ignoring valuable global information. Smaller top- k values ensure that the most relevant sub-prompts are employed, resulting in more robust and general performance across various degraded images.

Table 7. Abl. of General Prompts.

Method	PSNR \uparrow	SSIM \uparrow
w/o. General Prompts	31.52	0.9342
w/o. Depth-Anything [84]	31.67	0.9349
w. DINO [5]	31.77	0.9357
w. DINOv2 [57]	31.82	0.9359
w. Depth-Anything [84] (Ours)	31.99	0.9365
Length L_g	PSNR \uparrow	SSIM \uparrow
128 (General Prompts)	31.73	0.9354
192 (General Prompts)	31.88	0.9360
256 (General Prompts) (Ours)	31.99	0.9365
320 (General Prompts)	32.03	0.9365

Improvements of proposed General Prompts. Tab.7 illustrates the efficacy of incorporating the robust Depth-Anything [84] features as a constraint for general prompts. The depth-aware features intrinsic to Depth-Anything have demonstrated superior performance over other pre-trained models (e.g. DINO [5], DINOv2 [57]), particularly regarding scene understanding. Moreover, general prompts without such explicit constraints exhibit limitations in holistically background modeling.

Furthermore, our experiments revealed a performance bottleneck associated with increasing the number of general prompts. To optimize efficiency without compromising gains, we determine that selecting 256 tokens yields the

optimal balance, effectively avoiding unnecessary computational overhead.

Table 8. Com. of memory cost, PSNR, and SSIM across the different Depth-Anything [84] architectures.

Method	#Memory Cost	PSNR \uparrow	SSIM \uparrow
ViT-S-14 (Ours)	115.22 MB	31.99	0.9365
ViT-B-14	402.29 MB	31.96	0.9365
ViT-L-14	1314.38 MB	32.06	0.9366

Gains of different Depth-Anything Architecture. The ablation study shown in Tab.8 compares memory cost with image recovery quality of different Depth-Anything [84] architectures. We found that the ViT-S-14 model stands out for its low memory consumption of only 115.22 MB, while still achieving competitive PSNR and SSIM metrics for our final results. In comparison, ViT-B-14 and ViT-L-14 require significantly more memory with little corresponding gain in PSNR or SSIM.

Benefits of Contrast Prompt Loss (CPL). As shown in Tab.9, the CPL distinguishes designed prompts to guide the diffusion process. The table

Table 9. Abl. of Contrastive Prompt Loss (CPL).

Method	PSNR \uparrow	SSIM \uparrow
w/o. CPL	31.71	0.9350
w/o. Negative γ	31.81	0.9359
w/o. Positive γ	31.77	0.9358
w. CPL (Ours)	31.99	0.9365

shows that the pull of explicit constraints for prompts and the push of two prompts based on different motivations play an important role in improving the learning effect. They improve the guidance performance of conditions on diffusion by promoting enhanced representation learning. More ablation experiments can be found in the supplementary material.

7. Conclusion

This paper draws inspiration from the prompt learning and the concept of "Teaching Tailored to Talent", proposing a novel T³-DiffWeather. It utilizes weather-prompts constructed from free combinations of sub-prompts, and general prompts constrained by Depth-Anything to provide rich information for the diffusion process from the degradation and background perspectives. Experimental results demonstrate that our method achieves SOTA performance on various synthetic and real-world data sets, with excellent computational efficiency.

Acknowledgements

This work is supported by the Guangzhou-HKUST(GZ) Joint Funding Program (No. 2023A03J0671), the National Natural Science Foundation of China (Grant No. 61902275), the Guangzhou Industrial Information and Intelligent Key Laboratory Project (No. 2024A03J0628), and Guangzhou-HKUST(GZ) Joint Funding Program (No. 2024A03J0618).

References

- [1] Yunhao Ba, Howard Zhang, Ethan Yang, Akira Suzuki, Arnold Pfahnl, Chethan Chinder Chandrappa, Celso M de Melo, Suya You, Stefano Soatto, Alex Wong, et al. Not just streaks: Towards ground truth for single image deraining. In *Euro-pean Conference on Computer Vision*, pages 723–740. Springer, 2022. 8
- [2] Bolun Cai, Xiangmin Xu, Kui Jia, Chunmei Qing, and Dacheng Tao. Dehazenet: An end-to-end system for single image haze removal. *IEEE Transactions on Image Processing*, 25(11):5187–5198, 2016. 2
- [3] Shidong Cao, Wenhao Chai, Shengyu Hao, and Gaoang Wang. Image reference-guided fashion design with structure-aware transfer by diffusion models. In *Proceedings of the IEEE/CVF Conference on Computer Vision and Pattern Recognition*, pages 3524–3528, 2023. 3
- [4] Shidong Cao, Wenhao Chai, Shengyu Hao, Yanting Zhang, Hangyue Chen, and Gaoang Wang. Diffashion: Reference-based fashion design with structure-aware transfer by diffusion models. *IEEE Transactions on Multimedia*, 2023. 3
- [5] Mathilde Caron, Hugo Touvron, Ishan Misra, Hervé Jégou, Julien Mairal, Piotr Bojanowski, and Armand Joulin. Emerging properties in self-supervised vision transformers. In *Proceedings of the IEEE/CVF international conference on computer vision*, pages 9650–9660, 2021. 6, 9
- [6] Wenhao Chai and Gaoang Wang. Deep vision multimodal learning: Methodology, benchmark, and trend. *Applied Sciences*, 12(13):6588, 2022. 3
- [7] Wenhao Chai, Xun Guo, Gaoang Wang, and Yan Lu. Stablevideo: Text-driven consistency-aware diffusion video editing. In *Proceedings of the IEEE/CVF International Conference on Computer Vision*, pages 23040–23050, 2023. 3
- [8] Haoyu Chen, Jinjin Gu, Yihao Liu, Salma Abdel Magid, Chao Dong, Qiong Wang, Hanspeter Pfister, and Lei Zhu. Masked image training for generalizable deep image denoising. In *Proceedings of the IEEE/CVF Conference on Computer Vision and Pattern Recognition*, pages 1692–1703, 2023. 4
- [9] Haoyu Chen, Jingjing Ren, Jinjin Gu, Hongtao Wu, Xuequan Lu, Haoming Cai, and Lei Zhu. Snow removal in video: A new dataset and a novel method. In *2023 IEEE/CVF International Conference on Computer Vision (ICCV)*, pages 13165–13176. IEEE, 2023. 2
- [10] Haoyu Chen, Wenbo Li, Jinjin Gu, Jingjing Ren, Haoze Sun, Xueyi Zou, Zhensong Zhang, Youliang Yan, and Lei Zhu. Low-res leads the way:

- Improving generalization for super-resolution by self-supervised learning. In *Proceedings of the IEEE/CVF Conference on Computer Vision and Pattern Recognition*, pages 25857–25867, 2024. 4
- [11] Liangyu Chen, Xin Lu, Jie Zhang, Xiaojie Chu, and Chengpeng Chen. Hinet: Half instance normalization network for image restoration. In *Proceedings of the IEEE/CVF Conference on Computer Vision and Pattern Recognition*, pages 182–192, 2021. 6
- [12] Liangyu Chen, Xiaojie Chu, Xiangyu Zhang, and Jian Sun. Simple baselines for image restoration. In *European Conference on Computer Vision*, pages 17–33. Springer, 2022. 7
- [13] Po-Yi Chen, Alexander H. Liu, Yen-Cheng Liu, and Yu-Chiang Frank Wang. Towards scene understanding: Unsupervised monocular depth estimation with semantic-aware representation. In *Proceedings of the IEEE/CVF Conference on Computer Vision and Pattern Recognition (CVPR)*, 2019. 5
- [14] Sixiang Chen, Tian Ye, Yun Liu, and Erkang Chen. Dual-former: Hybrid self-attention transformer for efficient image restoration. *arXiv preprint arXiv:2210.01069*, 2022. 6
- [15] Sixiang Chen, Tian Ye, Yun Liu, Erkang Chen, Jun Shi, and Jingchun Zhou. Snowformer: Scale-aware transformer via context interaction for single image desnowing. *arXiv preprint arXiv:2208.09703*, 2022. 2
- [16] Sixiang Chen, Tian Ye, Yun Liu, Taodong Liao, Yi Ye, and Erkang Chen. Msp-former: Multi-scale projection transformer for single image desnowing. *arXiv preprint arXiv:2207.05621*, 2022. 2
- [17] Sixiang Chen, Tian Ye, Jinbin Bai, Erkang Chen, Jun Shi, and Lei Zhu. Sparse sampling transformer with uncertainty-driven ranking for unified removal of raindrops and rain streaks. In *Proceedings of the IEEE/CVF International Conference on Computer Vision*, pages 13106–13117, 2023. 1, 2, 7, 8
- [18] Sixiang Chen, Tian Ye, Chenghao Xue, Haoyu Chen, Yun Liu, Erkang Chen, and Lei Zhu. Uncertainty-driven dynamic degradation perceiving and background modeling for efficient single image desnowing. In *Proceedings of the 31st ACM International Conference on Multimedia*, pages 4269–4280, 2023. 2
- [19] Wei-Ting Chen, Hao-Yu Fang, Jian-Jiun Ding, Cheng-Che Tsai, and Sy-Yen Kuo. Jstasr: Joint size and transparency-aware snow removal algorithm based on modified partial convolution and veiling effect removal. In *Computer Vision—ECCV 2020: 16th European Conference, Glasgow, UK, August 23–28, 2020, Proceedings, Part XXI 16*, pages 754–770. Springer, 2020. 1, 2, 7
- [20] Wei-Ting Chen, Hao-Yu Fang, Cheng-Lin Hsieh, Cheng-Che Tsai, I Chen, Jian-Jiun Ding, Sy-Yen Kuo, et al. All snow removed: Single image desnowing algorithm using hierarchical dual-tree complex wavelet representation and contradict channel loss. In *Proceedings of the IEEE/CVF International Conference on Computer Vision*, pages 4196–4205, 2021. 1
- [21] Wei-Ting Chen, Zhi-Kai Huang, Cheng-Che Tsai, Hao-Hsiang Yang, Jian-Jiun Ding, and Sy-Yen Kuo. Learning multiple adverse weather removal via two-stage knowledge learning and multi-contrastive regularization: Toward a unified model. In *Proceedings of the IEEE/CVF Conference on Computer Vision and Pattern Recognition*, pages 17653–17662, 2022. 1, 2, 6, 7
- [22] Xiang Chen, Hao Li, Mingqiang Li, and Jinshan Pan. Learning a sparse transformer network for effective image deraining. In *Proceedings of the IEEE/CVF Conference on Computer Vision and Pattern Recognition*, pages 5896–5905, 2023. 1, 2
- [23] Zheng Chen, Yulun Zhang, Jinjin Gu, Xin Yuan, Linghe Kong, Guihai Chen, and Xiaokang Yang. Image super-resolution with text prompt diffusion. *arXiv preprint arXiv:2311.14282*, 2023. 3
- [24] Bodong Cheng, Juncheng Li, Ying Chen, Shuyi Zhang, and Tiejong Zeng. Snow mask guided adaptive residual network for image snow removal. *arXiv preprint arXiv:2207.04754*, 2022. 2
- [25] Alexey Dosovitskiy, Lucas Beyer, Alexander Kolesnikov, Dirk Weissenborn, Xiaohua Zhai, Thomas Unterthiner, Mostafa Dehghani, Matthias Minderer, Georg Heigold, Sylvain Gelly, et al. An image is worth 16x16 words: Transformers for image recognition at scale. *arXiv preprint arXiv:2010.11929*, 2020. 4
- [26] Yuetong Fang, Ziqing Wang, Lingfeng Zhang, Jiahang Cao, Honglei Chen, and Renjing Xu. Spiking wavelet transformer. *arXiv preprint arXiv:2403.11138*, 2024. 3
- [27] Jianshu Guo, Wenhao Chai, Jie Deng, Hsiang-Wei Huang, Tian Ye, Yichen Xu, Jiawei Zhang, Jenq-Neng Hwang, and Gaoang Wang. Versat2i: Improving text-to-image models with versatile reward. *arXiv preprint arXiv:2403.18493*, 2024. 3
- [28] Lanqing Guo, Chong Wang, Wenhan Yang, Siyu Huang, Yufei Wang, Hanspeter Pfister, and Bihan Wen. Shadowdiffusion: When degradation prior meets diffusion model for shadow removal. In *Proceedings of the IEEE/CVF Conference on Computer Vision and Pattern Recognition*, pages 14049–14058, 2023. 2, 3

- [29] Jonathan Ho, Ajay Jain, and Pieter Abbeel. Denoising diffusion probabilistic models. *Advances in neural information processing systems*, 33:6840–6851, 2020. 1, 3
- [30] Jonathan Ho, Ajay Jain, and Pieter Abbeel. Denoising diffusion probabilistic models. *Advances in neural information processing systems*, 33:6840–6851, 2020. 2
- [31] Jinhui Hou, Zhiyu Zhu, Junhui Hou, Hui Liu, Huanqiang Zeng, and Hui Yuan. Global structure-aware diffusion process for low-light image enhancement. *Advances in Neural Information Processing Systems*, 36, 2024. 6
- [32] Phillip Isola, Jun-Yan Zhu, Tinghui Zhou, and Alexei A Efros. Image-to-image translation with conditional adversarial networks. In *Proceedings of the IEEE conference on computer vision and pattern recognition*, pages 1125–1134, 2017. 7
- [33] Menglin Jia, Luming Tang, Bor-Chun Chen, Claire Cardie, Serge Belongie, Bharath Hariharan, and Ser-Nam Lim. Visual prompt tuning. In *European Conference on Computer Vision*, pages 709–727. Springer, 2022. 2, 3
- [34] Huaizu Jiang, Gustav Larsson, Michael Maire Greg Shakhnarovich, and Erik Learned-Miller. Self-supervised relative depth learning for urban scene understanding. In *Proceedings of the european conference on computer vision (eccv)*, pages 19–35, 2018. 5
- [35] Hai Jiang, Ao Luo, Haoqiang Fan, Songchen Han, and Shuaicheng Liu. Low-light image enhancement with wavelet-based diffusion models. *ACM Transactions on Graphics (TOG)*, 42(6):1–14, 2023. 6
- [36] Jingxia Jiang, Tian Ye, Jinbin Bai, Sixiang Chen, Wenhao Chai, Shi Jun, Yun Liu, and Erkang Chen. Five a network: You only need 9k parameters for underwater image enhancement. *arXiv preprint arXiv:2305.08824*, 2023. 3
- [37] Kui Jiang, Zhongyuan Wang, Peng Yi, Chen Chen, Zheng Wang, Xiao Wang, Junjun Jiang, and Chia-Wen Lin. Rain-free and residue hand-in-hand: A progressive coupled network for real-time image deraining. *IEEE Transactions on Image Processing*, 30: 7404–7418, 2021. 7
- [38] Zhongyu Jiang, Zhuoran Zhou, Lei Li, Wenhao Chai, Cheng-Yen Yang, and Jenq-Neng Hwang. Back to optimization: Diffusion-based zero-shot 3d human pose estimation. In *Proceedings of the IEEE/CVF Winter Conference on Applications of Computer Vision*, pages 6142–6152, 2024. 3
- [39] Yeying Jin, Aashish Sharma, and Robby T Tan. Dc-shadownet: Single-image hard and soft shadow removal using unsupervised domain-classifier guided network. In *Proceedings of the IEEE/CVF International Conference on Computer Vision*, pages 5027–5036, 2021. 3
- [40] Yeying Jin, Wending Yan, Wenhan Yang, and Robby T Tan. Structure representation network and uncertainty feedback learning for dense non-uniform fog removal. In *Asian Conference on Computer Vision*, pages 155–172. Springer, 2022. 1
- [41] Yeying Jin, Wenhan Yang, and Robby T Tan. Unsupervised night image enhancement: When layer decomposition meets light-effects suppression. In *European Conference on Computer Vision*, pages 404–421. Springer, 2022. 3
- [42] Yeying Jin, Beibei Lin, Wending Yan, Wei Ye, Yuan Yuan, and Robby T. Tan. Enhancing visibility in nighttime haze images using guided apsf and gradient adaptive convolution, 2023. 3
- [43] Yeying Jin, Wei Ye, Wenhan Yang, Yuan Yuan, and Robby T Tan. Des3: Adaptive attention-driven self and soft shadow removal using vit similarity. In *Proceedings of the AAAI Conference on Artificial Intelligence*, pages 2634–2642, 2024. 2, 3
- [44] Haoying Li, Yifan Yang, Meng Chang, Shiqi Chen, Huajun Feng, Zhihai Xu, Qi Li, and Yueting Chen. Srdiff: Single image super-resolution with diffusion probabilistic models. *Neurocomputing*, 479:47–59, 2022. 3
- [45] Ruoteng Li, Loong-Fah Cheong, and Robby T. Tan. Heavy rain image restoration: Integrating physics model and conditional adversarial learning. In *Proceedings of the IEEE/CVF Conference on Computer Vision and Pattern Recognition (CVPR)*, 2019. 7, 9
- [46] Ruoteng Li, Loong-Fah Cheong, and Robby T Tan. Heavy rain image restoration: Integrating physics model and conditional adversarial learning. In *Proceedings of the IEEE/CVF conference on computer vision and pattern recognition*, pages 1633–1642, 2019. 7
- [47] Ruoteng Li, Robby T Tan, and Loong-Fah Cheong. All in one bad weather removal using architectural search. In *Proceedings of the IEEE/CVF Conference on Computer Vision and Pattern Recognition*, pages 3175–3185, 2020. 1, 2, 7
- [48] Xia Li, Jianlong Wu, Zhouchen Lin, Hong Liu, and Hongbin Zha. Recurrent squeeze-and-excitation context aggregation net for single image deraining. In *Proceedings of the European conference on computer vision (ECCV)*, pages 254–269, 2018. 7
- [49] Xinqi Lin, Jingwen He, Ziyang Chen, Zhaoyang Lyu, Ben Fei, Bo Dai, Wanli Ouyang, Yu Qiao, and Chao Dong. Diffbir: Towards blind image restoration with generative diffusion prior. *arXiv preprint arXiv:2308.15070*, 2023. 2, 3

- [50] Liu. Desnownet: Context-aware deep network for snow removal. *IEEE TIP*, 2018. 2, 7, 8
- [51] Xiaohong Liu, Yongrui Ma, Zhihao Shi, and Jun Chen. Griddehazenet: Attention-based multi-scale network for image dehazing. In *Proceedings of the IEEE/CVF International Conference on Computer Vision*, pages 7314–7323, 2019. 2
- [52] Xing Liu, Masanori Suganuma, Zhun Sun, and Takayuki Okatani. Dual residual networks leveraging the potential of paired operations for image restoration. In *Proceedings of the IEEE/CVF Conference on Computer Vision and Pattern Recognition*, pages 7007–7016, 2019. 7
- [53] Yun Liu, Zhongsheng Yan, Sixiang Chen, Tian Ye, Wenqi Ren, and Erkang Chen. Nighthazeforner: Single nighttime haze removal using prior query transformer. *arXiv preprint arXiv:2305.09533*, 2023. 2
- [54] Ziwei Luo, Fredrik K Gustafsson, Zheng Zhao, Jens Sjölund, and Thomas B Schön. Image restoration with mean-reverting stochastic differential equations. *arXiv preprint arXiv:2301.11699*, 2023. 9
- [55] Ziwei Luo, Fredrik K Gustafsson, Zheng Zhao, Jens Sjölund, and Thomas B Schön. Refusion: Enabling large-size realistic image restoration with latent-space diffusion models. In *Proceedings of the IEEE/CVF Conference on Computer Vision and Pattern Recognition*, pages 1680–1691, 2023. 6, 9
- [56] Alexander Quinn Nichol and Prafulla Dhariwal. Improved denoising diffusion probabilistic models. In *International Conference on Machine Learning*, pages 8162–8171. PMLR, 2021. 3, 8
- [57] Maxime Oquab, Timothée Darcet, Théo Moutakanni, Huy Vo, Marc Szafraniec, Vasil Khalidov, Pierre Fernandez, Daniel Haziza, Francisco Massa, Alaaeldin El-Nouby, et al. Dinov2: Learning robust visual features without supervision. *arXiv preprint arXiv:2304.07193*, 2023. 5, 6, 9
- [58] Yichen Ouyang, Wenhao Chai, Jiayi Ye, Dapeng Tao, Yibing Zhan, and Gaoang Wang. Chasing consistency in text-to-3d generation from a single image. *arXiv preprint arXiv:2309.03599*, 2023. 3
- [59] Ozan Özdenizci and Robert Legenstein. Restoring vision in adverse weather conditions with patch-based denoising diffusion models. *IEEE Transactions on Pattern Analysis and Machine Intelligence*, 2023. 1, 2, 3, 5, 7, 8, 9
- [60] Vaishnav Potlapalli, Syed Waqas Zamir, Salman Khan, and Fahad Shahbaz Khan. Promptir: Prompting for all-in-one blind image restoration. *arXiv preprint arXiv:2306.13090*, 2023. 2, 3, 5, 9
- [61] Rui Qian, Robby T Tan, Wenhan Yang, Jiajun Su, and Jiaying Liu. Attentive generative adversarial network for raindrop removal from a single image. In *Proceedings of the IEEE conference on computer vision and pattern recognition*, pages 2482–2491, 2018. 2, 7
- [62] Yuwei Qiu, Kaihao Zhang, Chenxi Wang, Wenhan Luo, Hongdong Li, and Zhi Jin. Mb-taylorformer: Multi-branch efficient transformer expanded by taylor formula for image dehazing. In *Proceedings of the IEEE/CVF International Conference on Computer Vision*, pages 12802–12813, 2023. 2
- [63] Ruijie Quan, Xin Yu, Yuanzhi Liang, and Yi Yang. Removing raindrops and rain streaks in one go. In *Proceedings of the IEEE/CVF Conference on Computer Vision and Pattern Recognition*, pages 9147–9156, 2021. 2, 7, 8
- [64] Yuhui Quan, Shijie Deng, Yixin Chen, and Hui Ji. Deep learning for seeing through window with raindrops. In *Proceedings of the IEEE/CVF International Conference on Computer Vision*, pages 2463–2471, 2019. 7
- [65] Alec Radford, Jong Wook Kim, Chris Hallacy, Aditya Ramesh, Gabriel Goh, Sandhini Agarwal, Girish Sastry, Amanda Askell, Pamela Mishkin, Jack Clark, et al. Learning transferable visual models from natural language supervision. In *International conference on machine learning*, pages 8748–8763. PMLR, 2021. 3
- [66] Dongwei Ren, Wangmeng Zuo, Qinghua Hu, Pengfei Zhu, and Deyu Meng. Progressive image de-raining networks: A better and simpler baseline. In *Proceedings of the IEEE/CVF Conference on Computer Vision and Pattern Recognition*, pages 3937–3946, 2019. 2
- [67] Hongwei Ren, Yue Zhou, Jiadong Zhu, Haotian Fu, Yulong Huang, Xiaopeng Lin, Yuetong Fang, Fei Ma, Hao Yu, and Bojun Cheng. Rethinking efficient and effective point-based networks for event camera classification and regression: Eventmamba. *arXiv preprint arXiv:2405.06116*, 2024. 3
- [68] Robin Rombach, Andreas Blattmann, Dominik Lorenz, Patrick Esser, and Björn Ommer. High-resolution image synthesis with latent diffusion models. In *Proceedings of the IEEE/CVF conference on computer vision and pattern recognition*, pages 10684–10695, 2022. 3
- [69] Chitwan Saharia, Jonathan Ho, William Chan, Tim Salimans, David J Fleet, and Mohammad Norouzi. Image super-resolution via iterative refinement. *IEEE Transactions on Pattern Analysis and Machine Intelligence*, 45(4):4713–4726, 2022. 3
- [70] Karen Simonyan and Andrew Zisserman. Very deep convolutional networks for large-scale image recognition. *arXiv preprint arXiv:1409.1556*, 2014. 6

- [71] Enxin Song, Wenhao Chai, Guanhong Wang, Yucheng Zhang, Haoyang Zhou, Feiyang Wu, Haozhe Chi, Xun Guo, Tian Ye, Yanting Zhang, et al. Moviechat: From dense token to sparse memory for long video understanding. In *Proceedings of the IEEE/CVF Conference on Computer Vision and Pattern Recognition*, pages 18221–18232, 2024. 3
- [72] Enxin Song, Wenhao Chai, Tian Ye, Jenq-Neng Hwang, Xi Li, and Gaoang Wang. Moviechat+: Question-aware sparse memory for long video question answering. *arXiv preprint arXiv:2404.17176*, 2024. 3
- [73] Jiaming Song, Chenlin Meng, and Stefano Ermon. Denoising diffusion implicit models. *arXiv preprint arXiv:2010.02502*, 2020. 7
- [74] Yang Song and Stefano Ermon. Improved techniques for training score-based generative models. *Advances in neural information processing systems*, 33:12438–12448, 2020. 8
- [75] Yuda Song, Zhuqing He, Hui Qian, and Xin Du. Vision transformers for single image dehazing. *arXiv preprint arXiv:2204.03883*, 2022. 1, 2
- [76] Haoze Sun, Wenbo Li, Jianzhuang Liu, Haoyu Chen, Renjing Pei, Xueyi Zou, Youliang Yan, and Yujia Yang. Coser: Bridging image and language for cognitive super-resolution. In *Proceedings of the IEEE/CVF Conference on Computer Vision and Pattern Recognition*, pages 25868–25878, 2024. 3
- [77] Jeya Maria Jose Valanarasu, Rajeev Yasarla, and Vishal M Patel. Transweather: Transformer-based restoration of images degraded by adverse weather conditions. In *Proceedings of the IEEE/CVF Conference on Computer Vision and Pattern Recognition*, pages 2353–2363, 2022. 1, 2, 5, 7
- [78] Tianyu Wang, Xin Yang, Ke Xu, Shaozhe Chen, Qiang Zhang, and Rynson WH Lau. Spatial attentive single-image deraining with a high quality real rain dataset. In *Proceedings of the IEEE/CVF Conference on Computer Vision and Pattern Recognition*, pages 12270–12279, 2019. 7
- [79] Ziqing Wang, Yuetong Fang, Jiahang Cao, Qiang Zhang, Zhongrui Wang, and Renjing Xu. Masked spiking transformer. In *Proceedings of the IEEE/CVF International Conference on Computer Vision*, pages 1761–1771, 2023. 3
- [80] Haiyan Wu, Yanyun Qu, Shaohui Lin, Jian Zhou, Ruizhi Qiao, Zhizhong Zhang, Yuan Xie, and Lizhuang Ma. Contrastive learning for compact single image dehazing. In *Proceedings of the IEEE/CVF Conference on Computer Vision and Pattern Recognition*, pages 10551–10560, 2021. 2, 6
- [81] Hongtao Wu, Yijun Yang, Haoyu Chen, Jingjing Ren, and Lei Zhu. Mask-guided progressive network for joint raindrop and rain streak removal in videos. In *Proceedings of the 31st ACM International Conference on Multimedia*, pages 7216–7225, 2023. 2
- [82] Bin Xia, Yulun Zhang, Shiyin Wang, Yitong Wang, Xinglong Wu, Yapeng Tian, Wenming Yang, and Luc Van Gool. Diffir: Efficient diffusion model for image restoration. *arXiv preprint arXiv:2303.09472*, 2023. 2
- [83] Jie Xiao, Xueyang Fu, Aiping Liu, Feng Wu, and Zheng-Jun Zha. Image de-raining transformer. *IEEE Transactions on Pattern Analysis and Machine Intelligence*, 2022. 1, 2, 7
- [84] Lihe Yang, Bingyi Kang, Zilong Huang, Xiaogang Xu, Jiashi Feng, and Hengshuang Zhao. Depth anything: Unleashing the power of large-scale unlabeled data. *arXiv preprint arXiv:2401.10891*, 2024. 2, 5, 6, 7, 9, 10
- [85] Tao Yang, Peiran Ren, Xuansong Xie, and Lei Zhang. Pixel-aware stable diffusion for realistic image super-resolution and personalized stylization. *arXiv preprint arXiv:2308.14469*, 2023. 3
- [86] Wenhan Yang, Robby T Tan, Jiashi Feng, Jiaying Liu, Zongming Guo, and Shuicheng Yan. Deep joint rain detection and removal from a single image. In *Proceedings of the IEEE conference on computer vision and pattern recognition*, pages 1357–1366, 2017. 2
- [87] Yijun Yang, Angelica I Aviles-Rivero, Huazhu Fu, Ye Liu, Weiming Wang, and Lei Zhu. Video adverse-weather-component suppression network via weather messenger and adversarial back-propagation. In *Proceedings of the IEEE/CVF International Conference on Computer Vision*, pages 13200–13210, 2023. 2
- [88] Yijun Yang, Hongtao Wu, Angelica I Aviles-Rivero, Yulun Zhang, Jing Qin, and Lei Zhu. Genuine knowledge from practice: Diffusion test-time adaptation for video adverse weather removal. *arXiv preprint arXiv:2403.07684*, 2024. 1
- [89] Tian Ye, Sixiang Chen, Yun Liu, Yi Ye, Jinbin Bai, and Erkang Chen. Towards real-time high-definition image snow removal: Efficient pyramid network with asymmetrical encoder-decoder architecture. In *Proceedings of the Asian Conference on Computer Vision*, pages 366–381, 2022. 2
- [90] Tian Ye, Yunchen Zhang, Mingchao Jiang, Liang Chen, Yun Liu, Sixiang Chen, and Erkang Chen. Perceiving and modeling density for image dehazing. In *European Conference on Computer Vision*, pages 130–145. Springer, 2022. 2
- [91] Tian Ye, Sixiang Chen, Jinbin Bai, Jun Shi, Chenghao Xue, Jingxia Jiang, Junjie Yin, Erkang Chen,

- and Yun Liu. Adverse weather removal with codebook priors. In *Proceedings of the IEEE/CVF International Conference on Computer Vision*, pages 12653–12664, 2023. 1, 2, 7, 9
- [92] Tian Ye, Sixiang Chen, Wenhao Chai, Zhaohu Xing, Jing Qin, Ge Lin, and Lei Zhu. Learning diffusion texture priors for image restoration. In *Proceedings of the IEEE/CVF Conference on Computer Vision and Pattern Recognition*, pages 2524–2534, 2024. 3
- [93] Syed Waqas Zamir, Aditya Arora, Salman Khan, Munawar Hayat, Fahad Shahbaz Khan, Ming-Hsuan Yang, and Ling Shao. Multi-stage progressive image restoration. In *Proceedings of the IEEE/CVF Conference on Computer Vision and Pattern Recognition*, pages 14821–14831, 2021. 7
- [94] Syed Waqas Zamir, Aditya Arora, Salman Khan, Munawar Hayat, Fahad Shahbaz Khan, and Ming-Hsuan Yang. Restormer: Efficient transformer for high-resolution image restoration. In *Proceedings of the IEEE/CVF conference on computer vision and pattern recognition*, pages 5728–5739, 2022. 7, 9
- [95] Kaihao Zhang, Rongqing Li, Yanjiang Yu, Wenhan Luo, and Changsheng Li. Deep dense multi-scale network for snow removal using semantic and depth priors. *IEEE Transactions on Image Processing*, 30: 7419–7431, 2021. 7
- [96] Ruofan Zhang, Jinjin Gu, Haoyu Chen, Chao Dong, Yulun Zhang, and Wenming Yang. Crafting training degradation distribution for the accuracy-generalization trade-off in real-world super-resolution. In *International conference on machine learning*, pages 41078–41091. PMLR, 2023. 4
- [97] Zhonghan Zhao, Wenhao Chai, Xuan Wang, Li Boyi, Shengyu Hao, Shidong Cao, Tian Ye, Jenq-Neng Hwang, and Gaoang Wang. See and think: Embodied agent in virtual environment. *arXiv preprint arXiv:2311.15209*, 2023. 3
- [98] Yu Zheng, Jiahui Zhan, Shengfeng He, Junyu Dong, and Yong Du. Curricular contrastive regularization for physics-aware single image dehazing. In *Proceedings of the IEEE/CVF Conference on Computer Vision and Pattern Recognition (CVPR)*, pages 5785–5794, 2023. 6
- [99] Kaiyang Zhou, Jingkang Yang, Chen Change Loy, and Ziwei Liu. Conditional prompt learning for vision-language models. In *Proceedings of the IEEE/CVF Conference on Computer Vision and Pattern Recognition (CVPR)*, pages 16816–16825, 2022. 3
- [100] Kaiyang Zhou, Jingkang Yang, Chen Change Loy, and Ziwei Liu. Learning to prompt for vision-language models. *International Journal of Computer Vision*, 130(9):2337–2348, 2022. 2, 3
- [101] Jun-Yan Zhu, Taesung Park, Phillip Isola, and Alexei A Efros. Unpaired image-to-image translation using cycle-consistent adversarial networks. In *Proceedings of the IEEE international conference on computer vision*, pages 2223–2232, 2017. 7
- [102] Lei Zhu, Zijun Deng, Xiaowei Hu, Chi-Wing Fu, Xuemiao Xu, Jing Qin, and Pheng-Ann Heng. Bidirectional feature pyramid network with recurrent attention residual modules for shadow detection. In *Proceedings of the European Conference on Computer Vision (ECCV)*, pages 121–136, 2018. 2
- [103] Yurui Zhu, Tianyu Wang, Xueyang Fu, Xuanyu Yang, Xin Guo, Jifeng Dai, Yu Qiao, and Xiaowei Hu. Learning weather-general and weather-specific features for image restoration under multiple adverse weather conditions. In *Proceedings of the IEEE/CVF Conference on Computer Vision and Pattern Recognition*, pages 21747–21758, 2023. 1, 2, 4, 5, 9